A Novel Compressive Sampling MRI Method Using Variable-Density k-Space Under-sampling and Substitution of Coefficients

HENRY KIRAGU*, ELIJAH MWANGI AND GEORGE KAMUCHA
School of Engineering
University of Nairobi
P.O. BOX 30197-00100, Nairobi
KENYA
hkiragu@mmu.ac.ke, elijah.mwangi@uonbi.ac.ke, gkamucha@uonbi.ac.ke

Abstract: - A fast Magnetic Resonance Imaging (MRI) algorithm that also reduces reconstruction artifacts is proposed in this paper. The method employs a variable-density k-space under-sampling scheme that reduces the image acquisition time. The under-sampled k-space is converted to an MR image that is corrupted by artifacts. The image is fully sampled using a sub-Gaussian random sampling matrix prior to being reconstructed in the Discrete Wavelet Transform (DWT) domain using a Compressive Sampling (CS) greedy method. The k-space coefficients that are acquired during the under-sampling step are used to replace their corresponding coefficients in the k-space of the compressively reconstructed image. Computer simulation test results are used to compare the performance of the proposed algorithm to other reported CS methods based on the Peak-Signal-to-Noise Ratio (PSNR) and the Structured SIMilarity (SSIM) measures. The results show that the proposed method yields an average PSNR improvement of 1.76 dB compared to the Orthogonal Matching Pursuit method (OMP). This translates to a 13% reduction in scan time for a given quality of the reconstructed image.

Key-Words: - Compressive sampling, variable-density, MRI, OMP, scan time, PSNR, k-space.

1 Introduction

A signal that has a concise representation in some suitable representation domain can be reconstructed from its measurement vector whose cardinality is less than the length of the signal. The paradigm used to under-sample and reconstruct such a signal is termed Compressive Sampling (CS) [1, 2, 3]. The CS methods reduce the acquisition time of a signal by sampling it at a sub-Nyquist rate prior to reconstruction using either optimization or iterative or Bayesian methods [3, 4]. Although Magnetic Resonance Imaging (MRI) has significant advantages over other medical imaging modalities, it suffers the drawbacks of long scan time as well as artifacts that compromise the quality of the image [5-7]. Magnetic Resonance (MR) images are usually sparse in the Discrete Fourier Transform (DFT) as well as the Discrete Wavelet Transform (DWT) domains and therefore, CS methods can be employed to reduce the scan time [5, 8].

A block-based CS technique is proposed in [9]. Although the method shows good results for parallel MRI, it is likely to have a high computational complexity when applied to conventional MRI because the sensed segments have to be re-combined. Qin and Guo [10] have proposed a compressive sensing MR image reconstruction scheme. The method incorporates Total Generalized Variation and Shearlet transform to compressively reconstruct images of high quality. The test results in the paper show that the method preserves the image features such as geometry, texture and smoothness. However, the quality of the reconstructed images is relatively low. For example, at 20% sampling rate, the average PSNR of the recovered image is 20.70 dB. In addition, the recovered images portray high inconsistencies in quality. This is evident from the large standard deviation of the PSNR of the reconstructed images which is 5.69 dB at 20% measurements.

A CS-MRI method that assumes smoothness and high correlation in MR images is proposed in [11]. For images of body organs such as the brain that possess localized lesions, the method is likely to fail since the images are neither smooth nor highly correlated. A CS method for fast recovery of images from limited samples is proposed in [12]. The specially designed sensing technique yielded high reconstruction speeds due to the possibility of obtaining the solution to the CS recovery problem in a closed form. The imaging acceleration is however achieved at the expense of the image quality. For example, the average SSIM index achieved at 25%

sampling ratio is 0.81 with a standard deviation of 0.035.

Unlike the methods reported in [9-12], the proposed algorithm presented in this paper employs a variable-density k-space sampling approach to reduce the scan time and a coefficients re-insertion step to improve the image quality. Use of the Haar wavelet transform and a greedy recovery algorithm reduces the computational cost of the method.

The rest of this paper is organized as follows: Section 2 gives an outline of the CS and MRI theory while the proposed algorithm is presented in section 3. Results and discussions are presented in Section 4 while Section 5 gives a conclusion and suggestions for future work.

2 Theoretical Background

2.1 Compressive Sampling Theory

The Compressive Sampling theory asserts that, an *N*-length signal that possesses a concise approximation in some suitable representation domain can be reconstructed from $M \ll N$ measurements. The signal is reconstructed as an *N*-length, *S*-sparse vector $\boldsymbol{x}$ in the representation domain. The under-sampled measurement of the signal $\boldsymbol{f}$ can be viewed as a measurement vector $\boldsymbol{y}$ given by;

$$\boldsymbol{y} = \boldsymbol{\Phi f}, \tag{1}$$

where $\boldsymbol{\Phi}$ is an $M \times N$ measurement matrix. The sparse signal $\boldsymbol{f}$ can be expanded in an orthonormal basis domain as follows:

$$\boldsymbol{f} = \sum_{i=1}^{N} x_i \psi_i = \boldsymbol{\Psi x}, \tag{2}$$

where $\boldsymbol{\Psi}$ is an $N \times N$ representation matrix. The sparse representation of the signal and the measurement vector $\boldsymbol{y}$ are therefore related by;

$$\boldsymbol{y} = \boldsymbol{Ax}, \tag{3}$$

where $\boldsymbol{A} = \boldsymbol{\Phi\Psi}$ is an $M \times N$ sensing matrix that is also referred to as the dictionary [2, 5, 8]. In order to reduce the number of measurements required to reconstruct the vector $\boldsymbol{x}$, the sensing matrix must posses low coherence. For all the sparse signals in a desired class to be uniquely reconstructed from their noisy measurements using CS methods, the sensing matrix must obey the Restricted Isometry Property (RIP). The matrix is said to obey the RIP if there exists a constant $\delta_s \geq 0$ which makes the following inequality to hold.

$$(1 - \delta_s)\|\boldsymbol{x}\|_2^2 \leq \|\boldsymbol{Ax}\|_2^2 \leq (1 + \delta_s)\|\boldsymbol{x}\|_2^2, \tag{4}$$

where δ_s is termed the isometry constant of order *s* of the matrix and $\|.\|_2^2$ denotes the square of the Euclidean norm. Equation (3) is under-determined and ill-posed. Therefore, a unique solution can only be obtained if the sparsity of vector $\boldsymbol{x}$ is invoked. The tractable methods used to obtain an approximate solution for vector $\boldsymbol{x}$ fall under the optimization, greedy or Bayesian categories.

The optimization methods include the l_1-minimization and the Least Absolute Shrinkage and Selection Operator (LASSO) methods. The l_1-minimization method involves approximation of the *S*-sparse signal by solving the following convex-relaxed problem.

$$\text{minimize}\|\boldsymbol{x}\|_1 \text{ subject to } \boldsymbol{y} = \boldsymbol{Ax} \tag{5}$$

The LASSO method estimates the coefficients of a noisy sparse signal by solving the following least-squares problem;

$$\text{minimize}\|\boldsymbol{y} - \boldsymbol{Ax}\|_2^2 \text{ subject to } \|\boldsymbol{x}\|_1 \leq \tau, \tag{6}$$

where τ is a regularisation parameter that is dependent on the noise variance [1, 3, 5, 7].

Although the convex optimization techniques are powerful tools for solving sparse signals problems, greedy or iterative methods can also be used to solve such problems. These algorithms rely on iterative approximation of the signal coefficients and the support. This is achieved either by iteratively identifying the support of the signal until a stopping convergence criterion is attained, or by obtaining an improved estimate of the sparse signal at every iteration. The methods generally have lower computational complexity than the convex optimization algorithms. The greedy methods that are commonly used in sparse signal recovery include the Matching Pursuit (MP) and its improvements. The improvements are such as the Orthogonal matching pursuit (OMP), Stagewise orthogonal matching pursuit (StOMP), Gradient pursuit (GP) and CoSaMP (COmpressive Sampling Matching Pursuit) algorithms [1, 4, 5].

The Iterative Hard Thresholding (IHT) is another approach that is applicable to CS signal recovery. The method is generally employed as an algorithm for determining solutions of nonlinear inverse problems. The IHT algorithm commences with an initial estimate of the signal vector. Next, a predetermined number of iterative hard thresholding steps are carried to obtain a sequence of improved signal estimates [7].

2.2 Magnetic Resonance Imaging

The Magnetic Resonance Imaging (MRI) is a non-invasive technique that employs non-ionizing Radio

Frequency (RF) signals to generate good contrast medical images. When a body slice that is subjected to a static magnetic field is selectively excited, a transverse magnetization $\boldsymbol{M}(x,y)$ is produced. The MRI equipment receiver coils detect a Free Induction Decay (FID) signal $S(k_x,k_y)$ that is related to $\boldsymbol{M}(x,y)$ by;

$$S(k_x,k_y) = \int_{-F_y/2}^{F_y/2}\int_{-F_x/2}^{F_x/2} \boldsymbol{M}(x,y)\mathrm{e}^{-\mathrm{j}2\pi[k_x(t)x\ +k_y(t)y]}dxdy \quad (7)$$

where $k_x(t)$ and $k_y(t)$ are spatial frequency components in the read-out and phase-encoding directions respectively while F_x and F_y are the fields of view in the *x* and *y* directions respectively.

The MR image is constructed from a set of sampled measurements of the FID signal using the two-dimensional Inverse Discrete Fourier transform (2D-IDFT) [1, 13].

The FID signals are sampled in the spatial frequency domain at sampling periods of Δ_{k_x} and Δ_{k_y} with the highest spatial frequencies in the *x* and *y* directions being k_{xmax} and k_{ymax} respectively, to yield the signal

$$\mathcal{S}(u,v) = S(u\Delta_{k_x}, v\Delta_{k_y}) \quad (8)$$

where $u \in [(-N_r/2+1), N_r/2]$, $v \in [(-N_p/2+1), N_p/2]$, N_r is the number of read-out samples per acquisition and N_p is the number of phase encoding gradient steps. The reconstructed image ***I(a, b)*** is given by the inverse 2D-DFT of $\mathcal{S}(u,v)$ as follows;

$$\boldsymbol{I}(a,b) = \sum_{u=-N_r/2+1}^{u=N_r/2}\sum_{v=-N_p/2+1}^{v=N_p/2} \mathcal{S}(u,v)e^{j2\pi(\frac{au}{N_r}+\frac{bv}{N_p})} \quad (9)$$

where $a \in [(-N_r/2+1), N_r/2]$ and $b \in [(-N_p/2+1),\ N_p/2]$ [1, 5, 13, 14].

One of the demerits associated with MRI include the presence of patient-related as well as equipment-related artifacts in the MR images. The artifacts together with noise compromise the quality of an MR image and may lead to a mis-diagnosis of a medical condition. Another disadvantage is the excessively lengthy image acquisition time. For example, the conventional Spin Echo (CSE) MRI has a scan time that is given by;

$$T_s = (TR)(N_p)(NEX) \quad (10)$$

where T_s is the scan time, *TR* is the pulse repetition time, N_p is the number of phase encoding gradient steps and *NEX* is the number of excitations per scan. By decreasing N_p, the image acquisition time is reduced proportionately [13, 14].

2.3 Image Quality Measures

Two of the commonly used image objective quality metrics are the Peak Signal to Noise Ratio (PSNR) and the Structural SIMilarity (SSIM) index. The PSNR of a $P\times Q$ pixels reconstructed image $\boldsymbol{g}$ is given by;

$$PSNR = 10\log_{10}\left(\frac{PQL^2}{\sum_{i=1}^{P}\sum_{j=1}^{Q}[\boldsymbol{z}-\boldsymbol{g}]^2}\right) \quad (11)$$

where $\boldsymbol{z}$ is the ground-truth image and L is the maximum pixel intensity value in $\boldsymbol{z}$. Although the PSNR measure does not match well with the characteristics of the Human Visual System (HVS), it has the advantage of simplicity [1].

The Structural SIMilarity (SSIM) index agrees well with the image quality judgment of the HVS. The SSIM of a reconstructed image $\boldsymbol{g}$ relative to a ground-truth image $\boldsymbol{z}$ is given by;

$$SSIM(\boldsymbol{z},\boldsymbol{g}) = \frac{(2\mu_z\mu_g + C_1)(2\sigma_{zg} + C_2)}{(\mu_z^2 + \mu_g^2 + C_1)(\sigma_z^2 + \sigma_g^2 + C_2)} \quad (12)$$

where the parameters μ_g and μ_z denote the means of the reconstructed and ground-truth images respectively. The parameters σ_g and σ_z denote the standard deviations of the reconstructed and ground-truth images respectively while σ_{zg} is the cross correlation between the two images. The constants C_1 and C_2 ensure that the value of $SSIM(\boldsymbol{z},\boldsymbol{g})$ does not approach an infinite value as the denominator of (12) becomes vanishingly small [1, 15].

3 Proposed Algorithm

A proposed fast CS-based method for MRI is presented in this section. The method uses a k-space under-sampling scheme that has a variable density that considerably reduces the MRI scan time. The imaging time reduction is achieved by using only a fraction of phase encoding gradient steps, N_p to capture enough data for reconstructing the MR image. The robustness of the method is enhanced by replacing some of the CS reconstructed k-space rows with the coefficients that were directly captured during the under-sampling stage.

The stages that constitute the proposed algorithm are illustrated in the block diagram shown in fig. 1. For each variable density under-sampled k-space acquisition, a fixed number of low-frequency rows at the centre of the k-space plus an equal number of evenly spaced high-frequency rows are captured. For example, to sample 50% (32 rows) of the k-space of a 64×32 pixels image, 16 rows are obtained from the centre of the k-space (rows 25 to 40). The other 16 rows (1, 4, 7, 10, 13, 16, 19, 22, 43, 46, 49, 52, 55, 58, 61 and 64) are selected to be evenly selected from either side of the picked central rows. This acquisition paradigm can be modelled as an element-wise product of the full k-space $\boldsymbol{S}(u,v)$ and a variable-density mask as;

$$\boldsymbol{S_u^{'}}(u,v) = \boldsymbol{S}(u,v).\boldsymbol{\mathcal{M}}(u,v) \quad (13)$$

where $\boldsymbol{S_u^{'}}(u,v)$ is the under-sampled k-space and $\boldsymbol{\mathcal{M}}(u,v)$ is a proposed mask given by;

$$\boldsymbol{\mathcal{M}}(u,v) = \begin{cases} 1 \quad \text{for } v \geq v_1\,, v \leq v_2 \text{ where } v_2 > v_1 \\ 0 \text{ for } v < v_1,\ v > v_2 \text{ and } \mathrm{mod}(v,q) = 0 \\ 0 \quad \text{elsewhere} \end{cases} \quad (14)$$

where $v \in (1,\ N_p)$, $u \in (1,\ N_r)$ and N_r is the number of read-out gradient steps [13]. For each measurement, the values of integers v_1, v_2 and q are selected to achieve the desired percentage measurement. For a 50% under-sampling, $v_1 = 25$, $v_2 = 40$ and $q = 3$. The Fourier domain under-sampled k-space is then converted into an MR image by taking the 2D-IDFT. This transformation reveals the coherent aliasing and Gibb's artifacts [1, 6]. The image is then re-shaped into a vector $\boldsymbol{f}^{'}$ prior to being fully sampled using a random Gaussian matrix $\boldsymbol{\Phi}$ to yield a measurement vector $\boldsymbol{y}^{'}$ as follows;

$$\boldsymbol{y}' = \boldsymbol{\Phi f}' \quad (15)$$

This random sampling converts the coherent artifacts in $\boldsymbol{f}^{'}$ into incoherent noise which is easier to denoise [6]. It also enables unique CS recovery in the DWT domain [4].

Next, the MR image is reconstructed from $\boldsymbol{y}^{'}$ in the DWT domain using the OMP method. This step compressively reconstructs the rows of $\boldsymbol{S}(u,v)$ that were not captured in $\boldsymbol{S_u^{'}}(u,v)$ during under-sampling [1, 5, 6]. The image is then converted into its k-space $\boldsymbol{S}^{''}(u,v)$ by determining the 2D-DFT. To reduce the artifacts and noise further, the non-zero k-space rows of $\boldsymbol{S_u^{'}}(u,v)$ that were captured in the first step of the algorithm are now inserted in $\boldsymbol{S}^{''}(u,v)$ to replace their corresponding CS reconstructed noisy rows to yield the output image k-space, $\boldsymbol{S_o}(u,v)$.

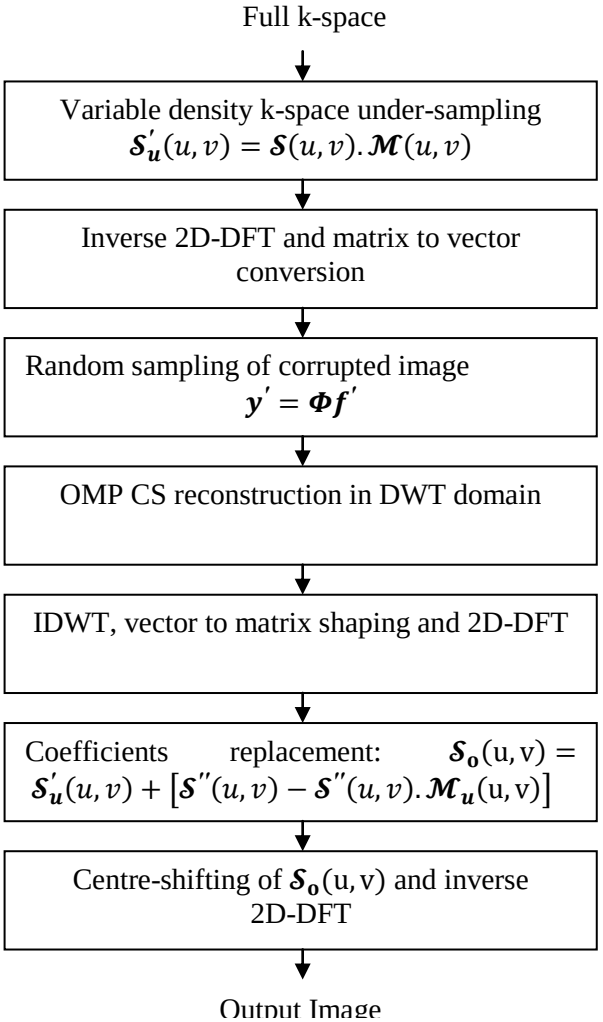

Fig.1. Block diagram of the proposed algorithm.

The rows substitution is accomplished as follows;

$$\boldsymbol{S_o}(u,v) = \boldsymbol{S_u^{'}}(u,v) + [\boldsymbol{S}^{''}(u,v) - \boldsymbol{S}^{''}(u,v).\boldsymbol{\mathcal{M}_u}(\mathrm{u,v})] \quad (16)$$

where $\boldsymbol{\mathcal{M}_u}(u,v)$ is a mask that is complementary to $\boldsymbol{\mathcal{M}}(u,v)$ and given by;

$$\boldsymbol{\mathcal{M}_u}(\mathrm{u,v}) = \mathrm{ones}(N_p\,, N_r) - \boldsymbol{\mathcal{M}}(\mathrm{u,v}) \quad (17)$$

where $\boldsymbol{S}^{''}(u,v).\boldsymbol{\mathcal{M}_u}(\mathrm{u,v})$ is the element-wise multiplication of $\boldsymbol{S}^{''}(u,v)$ by $\boldsymbol{\mathcal{M}_u}(\mathrm{u,v})$. Finally, the reconstructed image is generated by evaluating the 2D-IDFT of $\boldsymbol{S_o}(u,v)$.

To test the proposed method using MATLAB simulation, ground-truth MR images were converted into full k-spaces by taking the 2D-DFTs which were then subjected to the proposed algorithm.

4 Results and Discussions

To demonstrate the effectiveness of the proposed algorithm, MATLAB simulation results of thirty two images obtained from the MR image databases in [16-18] are presented here. All the images were first re-sized using bicubic interpolation prior to cropping them to a size of 64×32 pixels in order to use a sampling mask of the same size for all the images. The PSNR and SSIM metrics are used to assess the image reconstructed quality [1, 15].

In part (a) of fig. 2, a 64×32 pixels portion of a sagittal cross-section of a head ground-truth MR image is presented. An under-sampling mask that picks approximately 40% (26 rows) of the k-space is shown in part (b). The image reconstructed from the under-sampled k-space using the OMP method is presented in parts (c) and has a PSNR of 23.03 dB.
The image shown in part (d) was reconstructed using the proposed method. This image has a PSNR of 24.80 dB and is therefore of a better quality than the OMP reconstructed one.
Fig. 3 illustrates the stages of the proposed method using 50% measurements. Row (a) shows a 64×32 pixels ground-truth image for a portion of the pelvis and its full k-space matrix. At the left of row (b), the image reconstructed from the under-sampled k-space is presented. This image is corrupted by coherent artifacts and has a PSNR of 25.28 dB. The under-sampled k-space matrix is shown on the right of this image. The image reconstructed from the randomly sampled version of the image in part (b) using the OMP method is shown in part (c) together with its k-space. This image has a PSNR of 27.13 dB and exhibits high-frequency artifacts as is evident from a comparison of the k-spaces in parts (a) and (c). After re-insertion of the directly measured coefficients into the k-space of the image in part (c), the proposed method produces an image whose PSNR is 28.65 dB. This image plus the k-space matrix are presented in part (d). Inclusion of the coefficients re-insertion stage in the proposed method leads to an image quality which is better than that of conventional OMP.

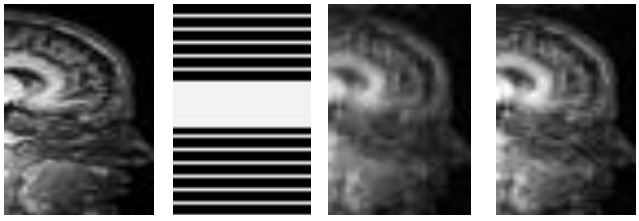

(a) (b) (c) (d)

Fig. 2. Comparison of the OMP and the proposed CS methods. (a) Ground-truth image. (b) A 40% sampling mask. (c) The OMP reconstructed image. (d) Image reconstructed using the proposed method.

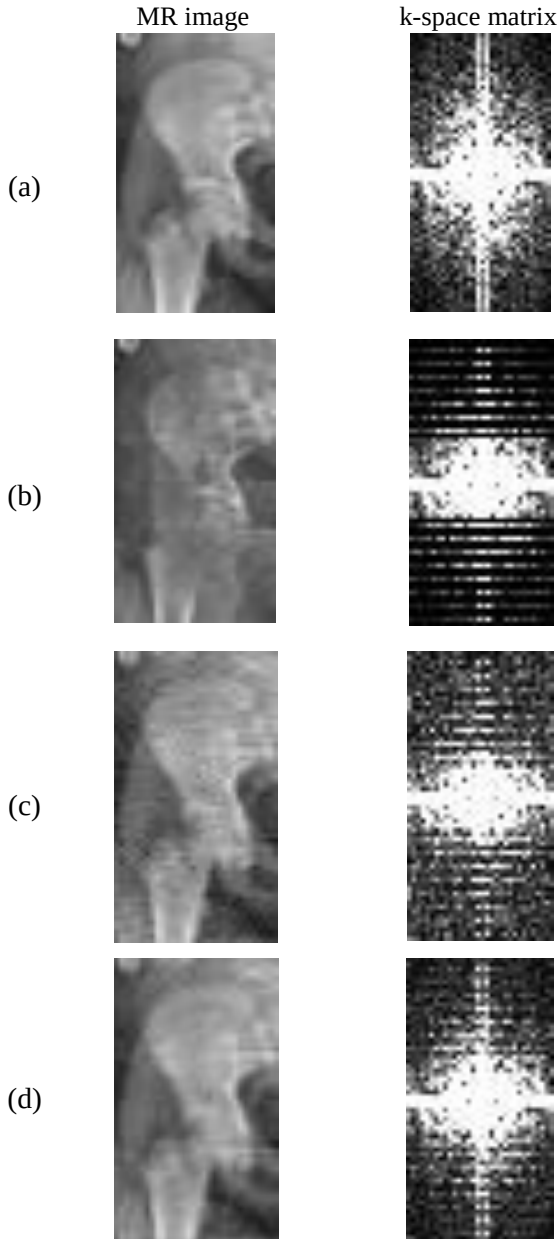

Fig. 3. Illustration of the proposed method. (a) Ground-truth image and k-space. (b) Under-sampled image and k-space. (c) OMP recovered image and k-space. (d) Proposed method recovered image and k-space.

Two MR images reconstructed using different CS methods at 40% measurements are shown in Fig. 4. The first row (a) shows the ground-truth images of blood vessels as well as a torso. Rows (b), (c) and (d) show the images reconstructed using the OMP, LASSO and the proposed methods respectively. The images reconstructed using the proposed method reveal the details better than those recovered using the other two methods.
In Table 1, the results of reconstruction of a thigh and a brain slice MR images using the proposed method and the LASSO method are shown. The k-spaces of the images were under-sampled at various percentage measurements.

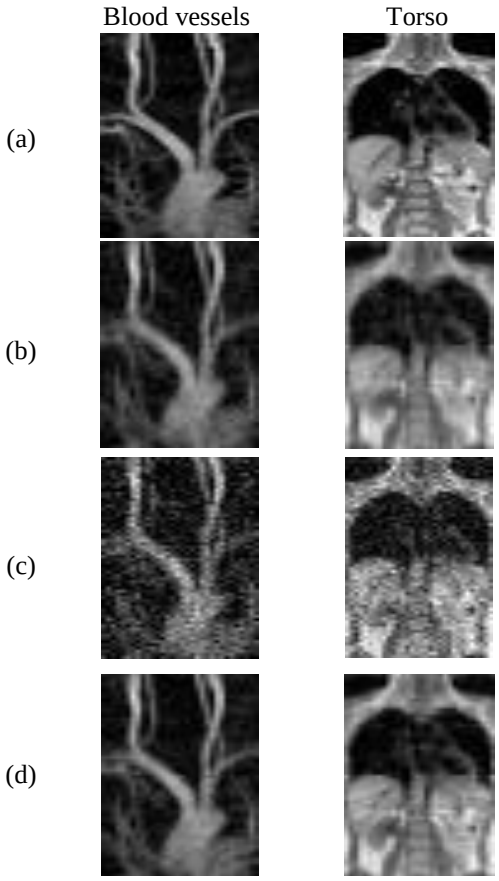

Fig. 4. Comparison. (a) Ground-truth MR image. (b) The OMP reconstruction. (c) The LASSO reconstruction. (d) Proposed method recovery.

The second-left column of the table presents the size of the measurement vector as a percentage of the image size. The third and fourth columns show the SSIM values of the reconstructed images using the LASSO and the proposed method respectively. The results show that the proposed method produced output images with higher SSIM index values than the LASSO optimization method for all the percentage measurements. Using the PSNR quality assessment index, similar results to those presented in table 1 were obtained. These results are as summarized in table 2. In the first column from the left, two ground-truth images are presented. They are images of parts of the pelvic bone and a shoulder. The second-left column presents the percentage measurements used. The third and fourth columns show the PSNR values of the images reconstructed using the OMP and the proposed methods respectively. From the table it is evident that the proposed method performs better than the OMP method. For example, at 30% measurements, the proposed method yields approximately 1.71 dB and 1.45 dB PSNR improvements over the OMP method for the pelvic bone and shoulder images respectively.

Table 1. The SSIM results of a thigh and a brain slice MR images

Input Image	Percentage Measurements (%)	LASSO SSIM	Proposed SSIM
	10	0.72	0.88
	20	0.81	0.95
	30	0.85	0.97
	40	0.85	0.98
	50	0.87	0.99
	60	0.89	0.99
	70	0.92	1.00
	10	0.61	0.81
	20	0.71	0.91
	30	0.77	0.94
	40	0.84	0.96
	50	0.85	0.97
	60	0.89	0.98
	70	0.90	0.99

Table 2. PSNR results for a pelvis and a shoulder images

MR Image	Percentage Measurements (%)	OMP PSNR(dB)	Proposed PSNR(dB)
	10	21.50	23.82
	20	25.88	26.47
	30	26.78	28.49
	40	27.50	29.28
	50	28.18	29.91
	60	28.81	30.41
	70	29.62	31.00
	10	16.32	17.83
	20	19.58	20.12
	30	19.97	21.42
	40	20.38	22.64
	50	23.73	25.65
	60	26.49	28.74
	70	28.37	30.04

A summary of the mean PSNR of the images reconstructed using three CS methods is presented graphically in part (a) of fig. 5. The proposed method produces images of higher quality than both the LASSO and OMP methods for all measurements. The average quality improvement of the proposed method at 30% or more measurements is 1.76 dB above the OMP method. This improvement translates to a 13% reduction in the scan-time for a given quality compared to the OMP method. For example, to reconstruct an image with a PSNR of 24.34 dB, the proposed algorithm and the OMP method require 30% and 43% of the full k-space respectively. In part (b) of fig. 5, the variance of the PSNR of the recovered images is presented. This summary shows that the proposed method has better reconstruction consistency than the other two. Similar results were obtained using the SSIM index.

(a)

(b)

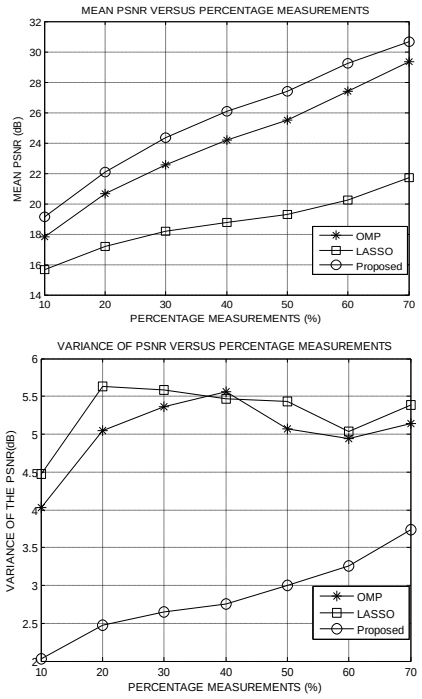

Fig. 5. Statistical summary. (a) Mean of PSNR. (b) Variance of PSNR.

5 Conclusion

A proposed CS-MRI algorithm has been presented in this paper. The algorithm reduces the imaging scan time by applying a variable-density k-space under-sampling technique. Substitution of some of the reconstructed k-space coefficients with the sampled ones was employed to improve the signal quality. Experimental results have been used to demonstrate that the proposed method reduces the MRI scan-time by 13 % compared to the OMP CS method. It also improves the image quality by an average PSNR of 1.76 dB for a given percentage measurement. Future work will focus on improving the under-sampling mask as well as the k-space substitution process.

References:

[1]Kiragu H, Mwangi E, Kamucha G. A Robust Compressive Sampling Method for MR Images Based on Partial Scanning and Apodization. *Proceedings of the IEEE ISSPIT*, Louisvlle, Kentucky, USA; Dec. 2018.

[2]Gnana F, John P, Sankararajan R. Efficient Reconstruction of Compressively Sensed Images and Videos Using Non-Iterative Method. *AEU-Intl. Journal of Electronics and Comm.*, Vol. 73, 2017, pp. 89-97.

[3]Jiang T, Zhang X, Li Y. Bayesian Compressive Sensing Using Reweighted Laplace Priors. *AEU-Intl. Journal of Electronics and Comm.*, Vol. 97, 2018, pp. 178-184.

[4]Yonina C. E, Kutyniok G. *Compressed sensing theory and applications*. 1st ed. Cambridge University Press, UK, 2015.

[5]Lustig M. *Sparse MRI*. PhD thesis. Stanford University, CA, USA, 2008.

[6]Vasanawala S. S, Alley M, Barth R, Hargreaves B, Pauly J, Lustig M. Faster Pediatric MRI via Compressed Sensing. *Proceedings on Annual Meeting of the SPR*, CA, USA; April 2009.

[7]Eslahi S. V, Dhulipala P. V, Shi C, Xie G, Ji J. X. Parallel Compressive Sensing in a Hybrid Space: Application in Interventional MRI. *Proc. of the Annual Intl. Conference of the IEEE EMBC*, Jeju Island, South Korea; July 2017.

[8]Kiragu H, Mwangi E, Kamucha G. A Hybrid MRI Method Based on Denoised CS and Detection of Dominant Coefficients. *Proc. of Intl. DSP conference*, London, UK; Aug. 2017.

[9]Mitra D, Zanddizari H, Rajan S. Improvement of Recovery in Segmentation-Based Parallel Compressive Sensing. *Proceedings of the IEEE ISSPIT*, Louisville, Kentucky, USA; Dec. 2018.

[10]Qin J, Guo W. An Efficient Compressive Sensing MR Image Reconstruction Scheme. *IEEE 10th Intl. Symp. Biomedical Imag.: nano to macro*, San Francisco, CA, USA; April 2013.

[11]Miyoshi T, Okuda M. Performance Comparison of MRI Restoration Methods with Low-Rank Priors. *Proceedings of the 7th IEEE GCCE*, Nara, Japan; Oct. 2018.

[12]Chun-Shien L, Hung-Wei C. Compressive Image Sensing for Fast Recovery From Limited Samples: A Variation on CS, *Elsevier Journal of Information Sciences*, Vol. 325, 2015, pp. 33–47.

[13]Nishimura D. G. *Principles of Magnetic Resonance Imaging*. Stanford University Press, USA, 2010.

[14]Hashemi R. H, Bradley W. G, Lisanti C. J. *MRI the Basics*. 3rd ed. Philadelphia: Lippincott Williams & Wilkins, USA, 2010.

[15]Wang, Z, Bovik, C. A universal image quality index, *IEEE Signal Proc. Letters*, Vol. 9, No. 3, 2002, pp. 81–84.

[16]Siemens Healthineers, *Dicom Images*, https:// www.healthcare.siemens.com/magnetic-resonance- imaging [Dec. 2018].

[17]Brown University, Rhode Island, USA. *MRI Research Facility*, https://www.brown. edu/ research/facilities/mri/, [Oct. 2018].

[18]Oregon Health and Science University, USA, *Diagnostic radiology*, https://www.ohsu.edu/xd/ education/schools/ school-of-medicine, [Sep. 2018].